Site preferences and formation energies of substitutional Si, Nb, Mo, Ta, and W solid solutions in $L1_0$ Ti-Al

C. Woodward* and S. Kajihara*
Materials and Manufacturing Directorate, Air Force Research Laboratory, Wright Patterson AFB, Ohio 45433

L. H. Yang
Physics H-Division, Lawrence Livermore National Laboratory, University of California, Livermore, California 94551
(Received 10 July 1997; revised manuscript received 13 January 1998)

Modifications to alloy chemistry are often used to tailor the intrinsic flow behavior of structural materials. Models of solution strengthening, high-temperature yield stress and creep must relate the effects of chemistry to the mechanisms which influence these material properties. In ordered alloys, additional information regarding the crystallographic site occupancy of substitutional solid solutions is required. The energy of intrinsic and substitutional point defects in $L1_0$ TiAl are calculated within a first principles, local density functional theory framework. We calculate the relaxed structures and energies of vacancies, antisites, and substitutional defects using a plane-wave pseudopotential method. The results of these total energy calculations are incorporated into a simple thermodynamic model in order to determine the density of point defects as a function of temperature and stoichiometry. Defect densities are presented as a function of alloy chemistry and temperature for binary TiAl and ternary additions (Si, Nb, Mo, Ta, and W). Defect formation energies are calculated using the derived chemical potentials of each atomic species for several alloy compositions. The predicted site selection of the solutes are in excellent agreement with recent x-ray emission experiments using a quantitative statistical method for atom location by channelling enhanced microanalysis. [S0163-1829(98)06818-0]

I. INTRODUCTION

The local density functional theory provides a robust framework for calculating the cohesive properties of a wide variety of materials. As methods and computational performance improve, it has become possible to accurately calculate an increasing number of intrinsic properties of metals and nonmetals. The advent of iterative diagonalization schemes for plane-wave psuedopotential methods have enabled calculations in semiconductors of surface reconstruction,[1] *ab initio* molecular dynamics,[2] and dislocation dissociation.[3] Existing conjugate-gradient methods have been extended to treat metals and have been applied to point defects[4] and grain boundaries[5] in simple metals and bulk properties in ordered intermetallics.[6] While partial band occupancy and multiple k-point sampling increase the complexity of the calculation, the iterative diagonalization method remains quite stable for even large supercells (larger than 100 atoms). Intermetallic alloys often require larger supercells and by their nature imply a multicomponent crystal bonding (i.e., metallic and covalent bonding).[7] The plane-wave basis is well suited for treating local and nonlocal bonding while at the same time permitting an efficient method for evaluating the Hellmann-Feynman forces. In this paper we use the conjugate-gradient plane-wave-pseudopotential method to study the electronic structure of point defects in $L1_0$ TiAl including the substitutional ternary elements Si, Nb, Mo, Ta, and W.

The TiAl alloys are representative of an emerging class of high-temperature structural materials. These materials are an attractive alternative for aerospace applications due to improvements in alloy density and flow behavior.[8] Alloy designers have taken great strides in moving from precipitation hardened multicomponent materials, the so-called superalloys, to intermetallic alloys such as TiAl and NiAl. In some cases the intermetallic alloys offer substantially better structural properties than superalloys.[9] However, the body of knowledge regarding these materials is still somewhat limited in comparison to the materials that are currently in service. Establishing a better fundamental understanding of the mechanisms that influence flow and fracture is needed.

It is well established that point defects can have a strong influence on the flow and fracture behavior of intermetallics. $B2$ NiAl and $L1_0$ TiAl have a strong dependence of yield stress with stoichiometry and alloy designers regularly use ternary additions to achieve solid solution strengthening.[9] For ordered alloys, additional information regarding the crystallographic site occupancy of ternary elements is required. In this work the sublattice site selection and the formation energy of ternary elements is estimated using defect energies that are calculated within the local density approximation. These energies include the relaxation of the lattice in the proximity of the point defect.

II. METHOD AND COMPUTATIONAL DETAILS

The point defects in TiAl are calculated using an iterative preconditioned conjugate-gradient method based on a plane-wave expansion for the electronic orbitals and a pseudopotential representation of the electron ion interactions.[10] This method, originally introduced by Teter *et al.*, has been extended to treat metals and has been used previously in calculations of the formation energies and lattice relaxation of point defects in Li and Al.[4] Convergence of the Kohn-Sham orbitals was achieved using charge density mixing and the

TABLE I. Cutoff radii (a.u.) for the pseudopotentials in this study.

Channel	Al	Si	Ti	Nb	Mo	Ta	W
s	1.80	1.90	2.48	2.48	2.48	2.42	2.45
p	2.00	1.90	2.96	2.89	2.89	2.88	2.84
d	2.00	1.90	2.13	1.98	1.88	1.51	1.86

positions of atoms surrounding the defect centers were optimized using a quasi-Newton method. The band-by-band optimization method for the electronic orbitals is well documented, other relevant details regarding this set of calculations are reviewed briefly below.

Pseudopotentials for this study were generated using the Troullier and Martins soft-core method.[11] The expansion in nonlocal components is truncated at $l=2$, with the *s* scattering channel being approximated by the local pseudopotential. Pseudopotentials are generated from the nonspin polarized valence ground state configurations. The cutoff radii for the different pseudopotentials used in this study are shown in Table I. This set of cutoff radii represents a balance between transferability of the pseudopotentials and the convergence of the cohesive energy within a plane-wave basis. The pseudopotentials are then cast in a fully separable form to minimize computational overhead in the supercell calculations.[12] In this study the Ti pseudopotential requires a plane-wave cutoff of approximately 60 Ry in order to converge the defect energies to better than 0.2 mRy. See, for example, Fig. 1. The other pseudopotentials (Al, Si, Mo, Nb, Ta, and W) can be run at smaller cutoffs ranging from 20–40 Ry. Gaussian broadening is used to perform the Brillouin zone energy integrations with Monkhorst-Pack special *k* points to sample the irreducible wedge in the first Brillouin zone.[13,14] A Gaussian broadening parameter of 0.030 Ry was employed throughout these calculations. The point defect calculations in TiAl are based on a 32 atom supercell with 6 special *k* points. The test calculations on the elastic moduli of TiAl and the simple bcc metals, described below, typically employed (8,8,8) *k*-point sampling grids. The exchange-correlation potential of Ceperley and Alder was employed for both the generation of the pseudopotentials and the supercell calculations.[15,16]

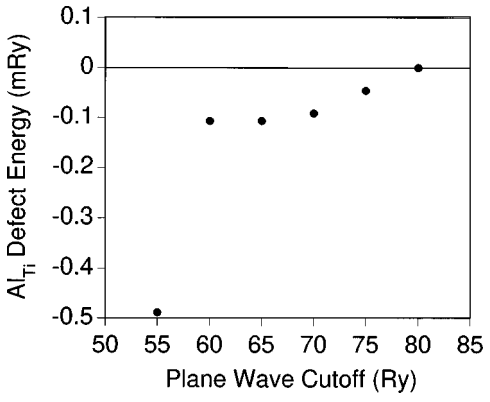

FIG. 1. Convergence of Al_{Ti} defect energy with plane-wave cutoff energy. The defect energy at a plane wave cutoff of 80 Ry is used as a reference energy.

In order to test the transferability of the pseudopotentials the logarithmic derivative of the pseudo and all electron atomic wave functions were compared. Also the lattice parameters, bulk modulus (K), and elastic constants were calculated for TiAl, Si, and the respective simple bcc metals. The lattice parameters and bulk modulus can be determined by fitting the energy as a function of hydrostatic strain to Murnaghan's equation of state (MES).[17] Similarly the elastic constants can be determined by applying symmetry-restricted strains to the lattice and fitting the energy dependence to second and fourth order polynomials. This procedure requires strains in excess of 5% of the lattice parameter.

An alternative procedure, which we have used here, is to evaluate the stress tensor for symmetry-restricted strains.[18–20] This has several advantages over traditional methods for determining the elastic constants.[21] First, smaller strains, which are within the elastic limit, can be employed. Typically these strains range from 0.2–0.5 % of the lattice constant. Second, far fewer calculations are needed because several C_{ij} can be determined from one strain tensor calculation. For example, to determine the C_{ij} of TiAl using traditional methods of fitting energy as a function of strain, approximately thirty energy minimization calculations are required.[21] Using the stress tensor only two calculations are required, including a third reference calculation for the unstrained lattice. Details of this method are described in Appendix A. The calculated lattice parameters, bulk moduli, and elastic constants for TiAl are shown in Table II. The elastic constants for TiAl were calculated using the traditional and stress tensor methods and we find good agreement between the two methods. The lattice constants and C_{ij} are in good agreement with previous local-density approximation (LDA) calculations and available experimental results.

Similar preliminary calculations were performed on Si, Mo, Nb, Ta, and W the results of which are presented in Table III. The elastic constants were calculated from the stress tensor and the bulk moduli were calculated two ways, using MES and the elastic constants. Lattice parameters are in good agreement with experimental results. The $E(\epsilon_{ij})$ (MES) results for the lattice constants are consistently larger than those predicted by the stress tensor. The bulk modulus derived from MES tends to fall between the experimental and the results derived from the elastic constants. The differences between the calculated and measured elastic constants are consistent with the results of other LDA studies on the elastic constants of metals.

III. RESULTS

The γ phase of TiAl is an ordered $L1_0$ fcc derivative structure consisting of alternating (001) layers of Ti and Al. The primitive cubic cell is body centered tetragonal and the conventional unit cell has the lattice parameters listed in Table II. We find the calculated band structure in very good agreement with previous full-potential linear muffin-tin-orbital (FP-LMTO) results.[32] Figures 2(a) and 2(b) show the characteristic d^2 and p-d hybrid bonding found in this intermetallic alloy. In the (001) plane consisting of Ti atoms there is hybrid d^2 bonding between nearest-neighbor Ti sites. Also, there is a p_z charge polarization about the Al site

TABLE II. Calculated equilibrium lattice parameters and elastic molduli (Mbar) for TiAl using the pseudopotentials in this study. The results of previous full potential LAPW and experimental studies are also included.

Method	a (a.u.)	c/a	K	C_{11}	C_{12}	C_{13}	C_{33}	C_{44}	C_{66}
E(ϵ_{ij})	7.484	1.026	1.25	1.77	0.99	0.93	1.81	1.11	0.85
$\sigma(\epsilon_{ij})$	7.460	1.020	1.20	1.71	0.96	0.91	1.75	1.11	0.84
FLAPW [a]	7.467	1.01	1.26	1.90	1.05	0.90	1.85	1.20	0.50
FLAPW [b]	7.372	1.037	1.27	1.88	0.98	0.96	1.90	1.26	1.00
FP-LMTO [c]			1.25	1.76	0.99	0.98	1.79	1.21	0.60
Exp. [d]	7.571 [e]	1.016 [e]	1.09	1.86	0.72	0.74	1.76	1.01	0.77
Exp. [f]	7.514	1.023	1.11	1.87	0.75	0.75	1.82	1.09	0.81

[a]Reference 22.
[b]Reference 21.
[c]Reference 23.
[d]Reference 24.
[e]Reference 25.
[f]Reference 26.

which has been linked to strong cohesion of the Al and Ti (001) planes. This is in excellent aggreement with previous full-potential linear augmented plane wave (FLAPW) and layered Korringa-Kohn-Rostoker (KKR) calculations.[33,34]

The structure and energy of the point defects were calculated in two steps. First the point defects were introduced into an otherwise perfect lattice represented by a 32-atom supercell. The self consistent electronic structure was calculated for this configuration using a plane-wave cutoff of 60 Ry. Next the positions of the first nearest-neighbor atoms were optimized using a quasi-Newton method until the vector components of the force on any atom was less than 1.0 $\times 10^{-3}$ Ry/Bohr. This converges the total energy to better than 0.3 mRy. Results for these calculations are shown in Table IV. The defect energies are defined as the energy difference between the defect cell and the perfect lattice. Optimizing the nearest-neighbor positions around the defect can reduce the defect energies by as much as 5 mRy. Changes in

TABLE III. Calculated equilibrium lattice parameters and elastic moduli for Si and the simple bcc metals using the pseudopotentials developed for this study. The results of previous electronic structure and experimental studies are included when available. Calculation of C_{44} in Si requires information regarding the internal strain parameter. These calculations gave the value shown in parentheses.

Property	Method	Si	Nb	Mo	Ta	W
	$E(\epsilon_{ij})$	10.1931	6.245	5.981	6.215	5.988
	$\sigma(\epsilon_{ij})$	10.1934	6.207	5.967	6.182	5.978
a (a.u.)	APW-MTA [a]		6.161	5.904	6.225	5.983
	FPLMTO [b]		6.139	5.879	6.070	5.879
	Exp. [c]	10.2659	6.2506	5.9486	6.228	5.974
	E(ϵ_{ij})	0.985	1.88	2.70	2.16	3.26
	$(C_{11}+2C_{12})/3$	0.953	1.97	2.81	2.23	3.24
K (Mbar)	APW-MTA [a]		1.948	2.881	2.008	3.256
	FPLMTO [b]		1.89	2.97	1.87	3.05
	Exp. [d]	0.992	1.73	2.70	1.93	3.14
C_{11} (Mbar)	$\sigma(\epsilon_{ij})$	1.62	2.87	4.70	3.04	5.33
	Exp. [d]	1.68	2.53	4.79	2.66	5.32
C_{12} (Mbar)	$\sigma(\epsilon_{ij})$	0.62	1.52	1.87	1.82	2.20
	Exp. [d]	0.650	1.33	1.65	1.58	2.05
C_{44} (Mbar)	$\sigma(\epsilon_{ij})$	0.88(0.58) [e]	0.21	1.01	0.66	1.43
	Exp. [d]	0.804	0.309	1.08	0.874	1.63

[a]Reference 28.
[b]Reference 29.
[c]Reference 30.
[d]Reference 31.
[e]Reference 27.

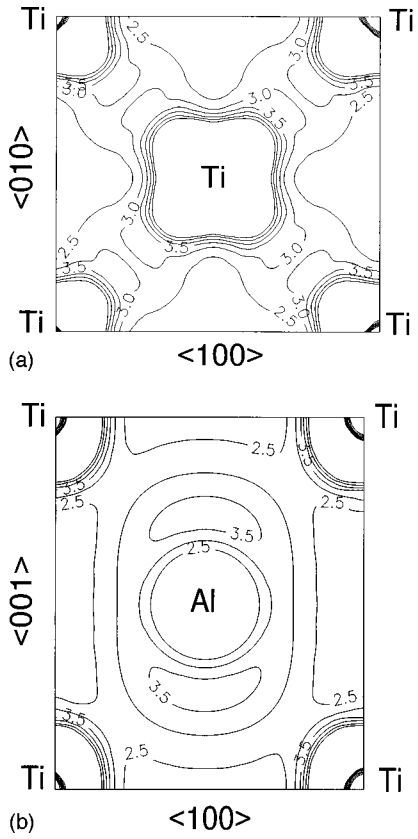

FIG. 2. Charge density contour plots of the (a) all Ti (001) plane and the (b) mixed (010) plane. Charge density is in units of 10^{-2} electron/a.u.^{3}

the defect energies of this magnitude can significantly affect the predicted density of thermal defects. In this study we assumed that the defect prefers the lattice site, no attempt was made to break the symmetry of the defect center. For some defects additional strain energy may be realized by relaxing the second and perhaps third nearest-neighbor atoms. However, in most of the cases considered in this work the lattice misfit is small and the strain energy from the second and third nearest-neighbor atoms will be less than 1 mRy. The displacement of the first nearest-neighbor atoms (Table IV) is typically less than 1% of the lattice constant. The magnitude of these strains is consistent with the strains used to calculate the elastic moduli for TiAl, Si, and the bcc metals described in the previous section.

IV. DISCUSSION

The defect energies presented in the results section, Table IV, give changes in the energy of the supercell which include changes in the alloy composition. In order to derive defect formation energies from these results some information regarding the chemical potentials for each chemical species is required. In general the formation energies and chemical potentials will be a function of temperature and composition. In this work we are particularly interested in how these quantities change with the stoichiometry of the host material. Constitutional defects are required for substitutional ternary solutes and for variations from stoichiometry. The chemical potentials and formation energies as defined by thermodynamics will reflect the changing requirements for constitutional defects as a function of composition.

TABLE IV. Defect energies (Ry) and the components of the displacement vectors of the representative nearest-neighbor atoms. The atoms are in the first quadrant with the defect site located at the origin. The vector components are in units of 10^{-3} of the respective lattice parameters a and c. The reference energy per atom of the perfect lattice is $E_{\mathrm{ref}} = -7.0021$ Ry.

	Defect energy		Nearest-neighbor displacement			
Defect	Unrelaxed	$\overline{R}_{\mathrm{ions}}$ optimized	R_x^{Ti}	R_z^{Ti}	R_x^{Al}	R_z^{Al}
V_{Al}	5.2850	5.2846	−1.09	−3.84	−0.82	0.00
V_{Ti}	8.9870	8.9830	−7.84	0.00	−3.02	−3.46
$\mathrm{Ti}_{\mathrm{Al}}$	−3.6837	−3.6842	0.70	−2.30	1.22	0.00
$\mathrm{Al}_{\mathrm{Ti}}$	3.7793	3.7727	−11.10	0.00	0.14	3.66
$\mathrm{Si}_{\mathrm{Al}}$	−4.0929	−4.0982	−4.78	−7.74	3.05	0.00
$\mathrm{Si}_{\mathrm{Ti}}$	−0.2765	−0.3042	−26.92	0.00	−0.91	6.16
$\mathrm{Nb}_{\mathrm{Al}}$	−8.8652	−8.8676	1.22	−5.49	4.65	0.00
$\mathrm{Nb}_{\mathrm{Ti}}$	−5.1845	−5.1856	0.37	0.00	0.32	0.44
$\mathrm{Mo}_{\mathrm{Al}}$	−15.9447	−15.9495	−2.02	−9.88	0.21	0.00
$\mathrm{Mo}_{\mathrm{Ti}}$	−12.2300	−12.2313	−4.94	0.00	−3.74	−0.90
$\mathrm{Ta}_{\mathrm{Al}}$	−8.9537	−8.9549	0.27	−2.86	1.87	0.00
$\mathrm{Ta}_{\mathrm{Ti}}$	−5.2620	−5.2619	0.03	0.00	−0.12	0.00
W_{Al}	−15.7657	−15.7717	−2.94	−10.62	−1.23	0.00
W_{Ti}	−12.0466	−12.0493	−4.44	0.00	−4.42	−1.81

In the ordered intermetallics there is an additional complexity, compared to the simple metals, in defining the defect formation energy as measured in the laboratory due to the constraints of chemical homogeneity. There is chemical driving force to keep the composition homogeneous in a given volume of material. This requires that thermal point defects form in ways that maintain the local composition. In a binary alloy there are four primitive excitations that satisfy this constraint: the double vacancy $V_\alpha + V_\alpha$, the double antisite $A_\beta + B_\alpha$, and two triple defects $2V_\alpha + A_\beta$ and $2V_\beta + B_\alpha$. Here the subscript refers to the sublattice on which the defect resides and V, A, and B refer to the vacancy, A and B atomic species, respectively. The point defects associated with these excitations are assumed to be noninteracting, so the effects of clustering or ordering are not considered. Ordered intermetallics that accomodate deviations from stoichiometry by forming $A_\beta(V_\beta)$ on the A rich side and $V_\alpha(B_\alpha)$ the B rich side are often called triple defect compounds. Triple defect mechanisms are known to dominate in several $B2$ intermetallics (NiAl, CoAl, and FeAl). In γ-TiAl the density of vacancies is small compared to deviations from stoichiometry and constitutional and thermal defects are dominated by the antisite mechanism.[35,36]

Recently, the thermodynamic properties of point defects in triple defect materials have been investigated in detail by several groups. Mayer *et al.* explored a grand canonical formalism for $B2$ FeAl using the defect energies calculated from a mixed-basis pseudopotential method in the local density approximation.[37] Analytic expressions and numerical solutions for the chemical potentials for a range of temperatures and composition were presented. At low temperatures

TABLE V. Expressions for the formation energies of point defects in terms of the chemical potentials and the defect energies in Table IV.

	Point defects					
	V_α	V_β	A_β	B_α	C_β	C_α
H_d	$E_\alpha^V+\mu_A$	$E_\beta^V+\mu_B$	$E_\beta^A+\mu_B-\mu_A$	$E_\alpha^B+\mu_A-\mu_B$	$E_\beta^C+\mu_B-\mu_C$	$E_\alpha^C+\mu_A-\mu_C$

the chemical potentials were found to change rapidly as the alloy composition changed from Fe to Al rich. The variation in chemical potentials with stoichiometry is consistent with the formation of different types of constitutional defects at these compositions. Using a different approach Mishin and Farkas developed identical analytical expressions for the chemical potentials and formation energies for point defects in $B2$ NiAl.[38] Also, Hagen and Finnis developed a slightly different formalism and applied it to $B2$ NiAl, yielding similar analytic expressions for the chemical potentials as a function of stoichiometry.[39] Defect energies from embedded atom simulations were used to illustrate trends in defect concentration as a function of temperature and composition. Fu and Yoo[40] also used a numerical thermodynamic model similar to that of Foiles and Daw[41] to study triple defects in NiAl and FeAl, using point defect energies calculated from a first-principles mixed basis method.

In order to predict the site occupancy of the various point defects at finite temperature we develop a numerical thermodynamic model similar to the one introduced by Foiles and Daw.[41] The free energy is minimized in the grand canonical ensemble to obtain the chemical potentials and the concentration of point defects. This is similar to the numerical models proposed by Mayer *et al.*[37] and Fu and Yoo,[40] however, we have extended the scheme to ternary systems. Extending the model to higher multicomponent systems (e.g., quaternary systems) is straightforward. For simplicity consider first a binary system such as γ-TiAl. Assume that the concentration of point defects is small so that the interaction of point defects can be neglected. The $L1_0$ lattice has two sublattices designated by α and β, and a total number of lattice sites N will be included in the ensemble. A and B designate the species that reside on the α and β sublattices in the perfect crystal. Each lattice site will be occupied by an atom of the appropriate species for that lattice site, a vacancy, or the other species. The thermal concentration of defects can be derived from an ensemble at fixed temperature and chemical potentials μ_i. In a binary alloy there are six unknowns to be determined: the density of the vacancies and antisites and the two chemical potentials. Minimizing the grand potential with respect to the density of thermal defects gives four equations for the density of thermal defects at equilibrium. The remaining two equations come from (1) defining the composition and (2) relating the Gibb's free energy to the chemical potentials at zero pressure. The input required to solve these equations are the Helmholtz energy of the perfect unit cell, the energy of the defect cells, and the desired composition at a given temperature. The resulting coupled equations can be solved by iteratively adjusting the chemical potentials until the required composition is obtained. A similar approach can be used to determine the density of substitutional ternary solutes. The numerical model, including details regarding solutions for ternary systems, is described in more detail in Appendix B. The current model is a slight improvement over the original work of Foiles and Daw in that the density of thermal defects is proportional to the partition function.

Many of the features of the binary alloy model can be illustrated analytically, this is also the case for the ternary systems. The energy of a grand canonical ensemble of N atom sites in an $L1_0$ lattice, for low temperature and zero pressure is

$$E=E_0+N_\alpha^v E_\alpha^v+N_\beta^v E_\beta^v+N_\alpha^B E_\alpha^B+N_\beta^A E_\beta^A+N_\alpha^C E_\alpha^C+N_\beta^C E_\beta^C. \tag{1}$$

The definition of the point defect formation energy is $H_d=(\partial E/\partial N_d)_{N_A,N_B,N_C}$. For a system consisting of N lattice sites a variation in the number of point defects will change N_A, N_B, or N_C. The free energy of the atomic species, written as the chemical potentials, are added to account for the changes in energy due to variations in the number of A, B, or C atoms:

$$\Omega=E_0+N_\alpha^v E_\alpha^v+N_\beta^v E_\beta^v+N_\alpha^B E_\alpha^B+N_\beta^A E_\beta^A+N_\alpha^C E_\alpha^C+N_\beta^C E_\beta^C -\mu_A N_A-\mu_B N_B-\mu_C N_C, \tag{2}$$

where

$$N_A=\frac{N}{2}-N_\alpha^v+N_\beta^A-N_\alpha^B-N_\alpha^C,$$

$$N_B=\frac{N}{2}-N_\beta^v+N_\alpha^B-N_\beta^A-N_\beta^C, \tag{3}$$

$$N_C=N_\alpha^C+N_\beta^C.$$

TABLE VI. Formation energies for the point defect complexes that preserve composition in the binary alloy. Expressions are evaulated using the calculated defect energies in Table IV and the energy of enthalpy per atom in the bulk material [e.g., $E_{\rm ref}=E_0/N=(\mu_A+\mu_B)/2$].

	Defect complex			
	$V_\alpha+V_\beta$	$A_\beta+B_\alpha$	$2V_\alpha+A_\beta$	$2V_\beta+B_\alpha$
$H_{\rm dc}$	$E_\alpha^V+E_\beta^V+2E_{\rm ref}$	$E_\alpha^B+E_\beta^A$	$2E_\alpha^V+E_\beta^A+2E_{\rm ref}$	$2E_\beta^V+E_\alpha^B+2E_{\rm ref}$
	3.582	1.204	4.593	3.775

TABLE VII. Expressions and numerical values for the μ_{Al} and μ_{Ti} (in Ry) for stioichiometric TiAl and for small deviations from stoichiometry. The numerical values are based on the defect energies presented in Table IV. Here the α and β subscripts refer to the Al and Ti sublattice, respectively.

	Ti rich	Composition stoichiometric	Al rich
μ_{Al}	$E_{\mathrm{ref}}-E_{\alpha}^{\mathrm{Ti}}/2$	$E_{\mathrm{ref}}+(E_{\beta}^{\mathrm{Al}}-E_{\alpha}^{\mathrm{Ti}})/4$	$E_{\mathrm{ref}}+E_{\beta}^{\mathrm{Al}}/2$
	-5.1600	-5.1379	-5.1158
μ_{Ti}	$E_{\mathrm{ref}}+E_{\alpha}^{\mathrm{Ti}}/2$	$E_{\mathrm{ref}}+(E_{\alpha}^{\mathrm{Ti}}-E_{\beta}^{\mathrm{Al}})/4$	$E_{\mathrm{ref}}-E_{\beta}^{\mathrm{Al}}/2$
	-8.8442	-8.8664	-8.8885

Taking the partial derivative with respect to the number of each defect gives the formal definition of the formation energy for each point defect. These are shown in Table V. The formation energy of the four primitive excitations that maintain the local composition, the vacancy pair, antisite pair, and triple defects can be expressed in terms of the defect energies and the energy/atom in the bulk ($E_0/N \equiv E_{\mathrm{ref}}$). The expressions for these formation energies are shown in Table VI, along with the respective numerical values predicted from the electronic structure calculations. The antisite pair mechanism has a significantly lower formation energy compared to the other defect mechanisms, therefore we expect antisites to dominate the thermal defects and constitutional defects in the binary alloy.

Following Mishin and Farkas[38] we express the total energy at zero temperature in terms of the energy/atom in the alloy u. Using the definition of the chemical potential $\mu_i = (\partial E/\partial N_i)_{N_i}$ and using the number densities for the concentration of species i:

$$\mu_A = u + n_A \frac{du}{dn_A}, \tag{4}$$

$$\mu_B = u - (1-n_A)\frac{du}{dn_A}. \tag{5}$$

Near stoichiometry $n_A = 0.5$ and $u = E_{\mathrm{ref}}$. We then write du/dn_A as $\delta u/\delta n_A$, where δu is the change in the energy/atom due to the formation of a single constitutional defect and δn_A is the respective change in alloy composition. As shown by Mishin and Farkas the two chemical potentials can then be expressed in terms of E_{ref}, δN_A, and δN_B. Introducing a constitutional defect, and expressing this change in composition as $\delta N_A + \delta N_B$,

$$\mu_A = \frac{\delta E_{\mathrm{site}}^{\mathrm{defect}} - 2E_{\mathrm{ref}}\delta N_B}{\delta N_A - \delta N_B}, \tag{6}$$

$$\mu_B = \frac{\delta E_{\mathrm{site}}^{\mathrm{defect}} - 2E_{\mathrm{ref}}\delta N_A}{\delta N_B - \delta N_A}. \tag{7}$$

For alloys dominated by antisite defects we need to consider two cases. An A-rich alloy will form N_{β}^{A} antisites and δN_A and δN_B will be $+1$ and -1, respectively. For a B-rich alloy, N_{α}^{B} antisites will give δN_A and δN_B equal to -1 and $+1$, respectively. This gives analytical expressions for the chemical potentials for compositions close to stoichiometry. The expressions and respective numerical values found in this study are shown in Table VII. Expressions for the chemical potentials at stoichoimetry are taken as the average of the chemical potentials found for the A-rich and B-rich alloys. The variation in chemical potential as a function of stoichiometry is consistent with the formation of constitutional defects as required for a given composition.

TABLE VIII. Expressions and numerical values for the formation energies of vacancies and antisites in γ-TiAl (in eV) for stoichiometric TiAl and for small deviations from stoichiometry. The numerical values are based on the defect energies presented in Table IV. Here the α and β subscripts refer to the Al and Ti sublattice, respectively.

	Ti rich	Composition stoichiometric	Al rich
V_{Al}	$E_{\mathrm{ref}}+E_{\alpha}^{V}-E_{\alpha}^{\mathrm{Ti}}/2$	$E_{\mathrm{ref}}+E_{\alpha}^{V}+(E_{\beta}^{\mathrm{Al}}-E_{\alpha}^{\mathrm{Ti}})/4$	$E_{\mathrm{ref}}+E_{\alpha}^{V}+E_{\beta}^{\mathrm{Al}}/2$
	1.695	1.995	2.296
V_{Ti}	$E_{\mathrm{ref}}+E_{\beta}^{V}+E_{\alpha}^{\mathrm{Ti}}/2$	$E_{\mathrm{ref}}+E_{\beta}^{V}+(E_{\alpha}^{\mathrm{Ti}}-E_{\beta}^{\mathrm{Al}})/4$	$E_{\mathrm{ref}}+E_{\beta}^{V}-E_{\beta}^{\mathrm{Al}}/2$
	1.888	1.587	1.286
$\mathrm{Al_{Ti}}$	$E_{\alpha}^{\mathrm{Ti}}+E_{\beta}^{\mathrm{Al}}$	$(E_{\alpha}^{\mathrm{Ti}}+E_{\beta}^{\mathrm{Al}})/2$	0.0
	1.204	0.602	0.0
$\mathrm{Ti_{Al}}$	0.0	$(E_{\alpha}^{\mathrm{Ti}}+E_{\beta}^{\mathrm{Al}})/2$	$E_{\alpha}^{\mathrm{Ti}}+E_{\beta}^{\mathrm{Al}}$
	0.0	0.602	1.204

Using these expressions for the chemical potentials we can evaluate the formation energy of the intrinsic point defects in γ-TiAl as a function of stoichiometry. The numerical values for the formation energies are shown in Table VIII. The derived formation energies reflect several constraints. In order for a finite density of constitutional defects to be present at low temperature the formation energy of these defects must approach zero. Also, the formation energy for the point defect excitations which maintain the local composition are independent of composition since these energies do not depend on the chemical potentials. Therefore, $H_{\alpha}^{V}+H_{\beta}^{V}$, $H_{\alpha}^{V}+H_{\beta}^{A}$, and $2H_{\alpha}^{V}+H_{\beta}^{A}$ are independent of stoichiometry.

The site selection of the ternary defects, at low temperature, can also be determined as a function of stoichiometry using the chemical potentials in Table VII. The difference in defect formation energy ($\delta H^{\mathrm{defect}} = H_{\alpha}^{\mathrm{defect}} - H_{\beta}^{\mathrm{defect}}$) are plotted in Fig. 3 as a function of stoichiometry. Here Ti rich and Al rich refer to alloys with $\mathrm{Ti_{Al}}$ and $\mathrm{Al_{Ti}}$ constitutional defects, respectively. Positive and negative values for $\delta H^{\mathrm{defect}}$ indicate that the β and α sublattice are prefered, respectively. The formal definitions of the chemical potential and formation energy for the ternary solutes imply that the formation energy for the prefered constitutional defect will be approximately equal to zero at low temperatures. This determines both the chemical potential and the formation energies for the solutes. The chemical potentials and formation energies of the various ternary solutes for low temperatures are

TABLE IX. Expressions and numerical values for the formation energies (in eV) and chemical potentials (in Ry) of ternary elements in γ-TiAl at low temperatures for compositions near stoichiometry. Changes in these quantities with alloy composition reflect the presence of different constitutional defects as designated in the table heading. The numerical values are based on the defects energies presented in Table IV. Here the α and β subscripts refer to the Al and Ti sublattice, respectively.

	Composition		
	Ti rich	Stoichiometric	Al rich
M_{Al}	$E_{\mathrm{ref}}+E_{\alpha}^{M}-E_{\alpha}^{\mathrm{Ti}}/2-\mu_M$	$E_{\mathrm{ref}}+E_{\alpha}^{M}+(E_{\beta}^{\mathrm{Al}}-E_{\alpha}^{\mathrm{Ti}})/4-\mu_M$	$E_{\mathrm{ref}}+E_{\alpha}^{M}+E_{\beta}^{\mathrm{Al}}/2-\mu_M$
M_{Ti}	$E_{\mathrm{ref}}+E_{\beta}^{M}+E_{\alpha}^{\mathrm{Ti}}/2-\mu_M$	$E_{\mathrm{ref}}+E_{\beta}^{M}+(E_{\alpha}^{\mathrm{Ti}}-E_{\beta}^{\mathrm{Al}})/4-\mu_M$	$E_{\mathrm{ref}}+E_{\beta}^{M}-E_{\beta}^{\mathrm{Al}}/2-\mu_M$
μ_{Si}	−9.2582	−9.2361	−9.2140
$\mathrm{Si_{Al}}$	0.0	0.0	0.0
$\mathrm{Si_{Ti}}$	1.4933	0.8922	0.2896
μ_{Nb}	−14.0298	−14.0519	−14.0741
$\mathrm{Nb_{Al}}$	0.0299	0.6310	1.2376
$\mathrm{Nb_{Ti}}$	0.0	0.0	0.0
μ_{Mo}	−21.1095	−21.0976	−21.1198
$\mathrm{Mo_{Al}}$	0.0	0.1387	0.7412
$\mathrm{Mo_{Ti}}$	0.4624	0.0	0.0
μ_{Ta}	−14.1149	−14.1282	−14.1504
$\mathrm{Ta_{Al}}$	0.0	0.4814	1.0934
$\mathrm{Ta_{Ti}}$	0.1197	0.0	0.0
μ_{W}	−20.9317	−20.9156	−20.9378
$\mathrm{W_{Al}}$	0.0	0.0816	0.6841
$\mathrm{W_{Ti}}$	0.5195	0.0	0.0

shown in Table IX as function of stoichiometry. Again, Ti rich and Al rich refer to alloys with $\mathrm{Ti_{Al}}$ and $\mathrm{Al_{Ti}}$ constitutional defects, respectively. The chemical potentials listed in Tables VII and IX are consistent with the chemical potentials found using the numerical model described in Appendix B. A small $\delta H^{\mathrm{defect}}$ (<0.1 eV$\approx 1200 k_B$) implies that at finite temperature the ternary will be shared between the two sublattices. However, ternary defects formed by thermal excitation are also required to maintain local chemistry. There are two primitive excitations that meet this requirement based on the exchange of a ternary defect between the two sublattices:

$$C_{\alpha} \rightleftharpoons B_{\alpha}+C_{\beta}, \tag{8}$$

$$C_{\beta} \rightleftharpoons A_{\beta}+C_{\alpha}. \tag{9}$$

The ternary exchange energies are easily evaluted since the composition remains constant. The equilibrium concentration of point defects associated with these defect mechanisms varies with temperature according to

$$\frac{n_{\alpha}^{B} n_{\beta}^{C}}{n_{\alpha}^{C}} = \exp\left(\frac{-(H_{\alpha}^{B}+H_{\beta}^{C}-H_{\alpha}^{C})}{k_B T}\right), \tag{10}$$

$$\frac{n_{\beta}^{A} n_{\alpha}^{C}}{n_{\beta}^{C}} = \exp\left(\frac{-(H_{\beta}^{A}+H_{\alpha}^{C}-H_{\beta}^{C})}{k_B T}\right), \tag{11}$$

where the formation energy for the two exchange mechanisms are given by

$$E_{C\alpha\rightarrow\beta} = E_{\alpha}^{B}+E_{\beta}^{C}-E_{\alpha}^{C}, \tag{12}$$

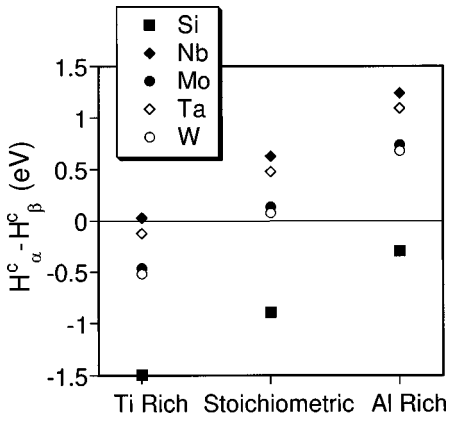

FIG. 3. The difference in formation energy of ternary substitutional defects (Al, Nb, Mo, Ta, and W) residing on different sublattices $\delta H^{\mathrm{defect}}=H_{\alpha}^{\mathrm{defect}}-H_{\beta}^{\mathrm{defect}}$ for compositions near stoichiometry in γ-TiAl.

TABLE X. Expressions and numerical values for the formation energies (in eV) of the ternary exchange defects as discussed in the text. The numerical values are based on the defect energies presented in Table IV. Here the α and β subscripts refer to the Al and Ti sublattice, respectively.

Defect complex		Ternary element				
Reaction	Formation energy	Si	Nb	Mo	Ta	W
$M_\alpha \rightleftharpoons \mathrm{Ti}_\alpha + M_\beta$	$E_\alpha^{\mathrm{Ti}} + E_\beta^M - E_\alpha^M$	1.493	−0.030	0.462	0.120	0.520
$M_\beta \rightleftharpoons \mathrm{Al}_\beta + M_\alpha$	$E_\beta^{\mathrm{Al}} + E_\alpha^M - E_\beta^M$	−0.290	1.234	0.741	1.084	0.684

$$E_{C\beta\to\alpha} = E_\beta^A + E_\alpha^C - E_\beta^C . \tag{13}$$

The ternary elements produce constitutional defects for any given temperature and underlying stoichiometry so the ratio of the defect concentrations can vary substantially. As a consequence the formation energy for the ternary exchange mechanisms can go to zero, or actually be less than zero. If the formation energy for a ternary exchange is small it will strongly influence the site selection of ternaries with a small $\delta H^{\mathrm{defect}}$. For example, Fig. 3 shows a small δH^{Nb} for Ti-rich TiAl. However, the ternary exchange which produces $\mathrm{Nb_{Ti}}$ has a low energy and is expected to dominate the thermally activated processes. Therefore, there will be little mixing of Nb between the two sublattices due to thermal activation at higher temperatures. The formation energies for the ternary exchange mechanisms for the various solutes, calculated from the data in Table IV, are shown in Table X.

The results from the numerical model described in Appendix B for binary TiAl at 1273 K are shown in Fig. 4. As expected the constitutional defects are dominated by antisites with the density of Al and Ti vacancies less than 10^{-6} throughout this range in composition. The density of vacancies is similar to that found in simple fcc metals. The formation of $\mathrm{Al_{Ti}}$ rather than $\mathrm{V_{Ti}}$ for Al-rich TiAl is consistent with the early experimental work of Elliot and Rostoker.[36] Phase diagrams for the binary alloy indicate that γ-TiAl occurs as a single phase in a range of 48–64 % Al for temperatures below 1600 K. The Ti-rich region has coexisting α and γ phases and compositions for the γ phase with less than 48% Al have have not been observed.

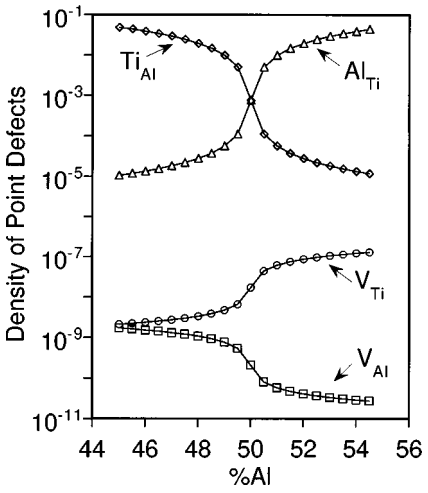

FIG. 4. Predicted point defect densities, at 1073 K, as a function of stoichiometry.

Results for the ternary additions in TiAl at 1273 K are shown in Figs. 5(a)–5(e). As expected from the data shown in Fig. 3, Si prefers the Al (α) sublattice for compositions ranging from 42–56 atomic percent Al while Nb prefers the Ti (β) sublattice. The site preference for Mo, Ta, and W depends on the stoichiometry of the host alloy. Figure 6 shows the dependence of site occupancy with stoichiometry for the five ternaries considered in this study for a ternary concentration of 1 at. % and a temperature of 1273 K.

Independent of the current study, Rossouw *et al.* have measured site occupancy using the transmission electron microscopy (TEM) x-ray spectroscopy technique of atom location by channelling-enhanced microanalysis (ALCHEMI) used in conjuction with a statistical multivariate method.[42] Standard ALCHEMI uses the differences and ratios of characteristic x-ray emission intensities for different fast electron channeling conditions to determine atom locations. Unfortunately, the results of standard ALCHEMI measurements are often difficult to reproduce. Rossouw *et al.* find that by adopting a statistical method the effects of systematic errors in the collected data can be minimized, and a quantitative estimate of the uncertainties in the results can be obtained. In their study of ternary additions in TiAl the composition of the γ phase could not be determined unambiguously using energy-dispersive x-ray analysis (EDXA).[42] The results of the current first principles study indicate that site selection of some of the ternary additions are quite sensitive to the underlying stoichiometry of the γ phase. An estimate of the composition of the γ phase is needed in order to compare the current results with experiment.

The initial ingots studied by Rossouw and co-workers had nominal compositions of $(\mathrm{Ti_{52}\text{-}Al_{48}})_{99}\text{-}M_1$, where M is the ternary impurity. These were then heat treated at 1473 K for six hours to produce a γ-α_2 duplex structure. The most recent studies of the TiAl binary phase diagram show the solvus line between the $\alpha_2+\gamma$ phase field and the γ phase at approximately 48.75% Al and 49% Al for the temperatures 1473 and 800 K, respectively.[43–45] Depending upon the cooling rates the compositions of the γ phase alloys could range from 48.75 to 49.00 at. % Al. Also, the presence of ternary elements can shift the solvus line from that found for the binary alloy. Figure 7 compares the experimental data of Rossouw *et al.* to the results of the current study assuming a composition of $(\mathrm{Ti_{51}\text{-}Al_{49}})_{99}\text{-}M_1$. The predicted results are in excellent agreement with experiment.

V. SUMMARY

The electronic structure of point defects in γ-TiAl, including the ternary elements Si, Nb, Mo, W, and Ta as sub-

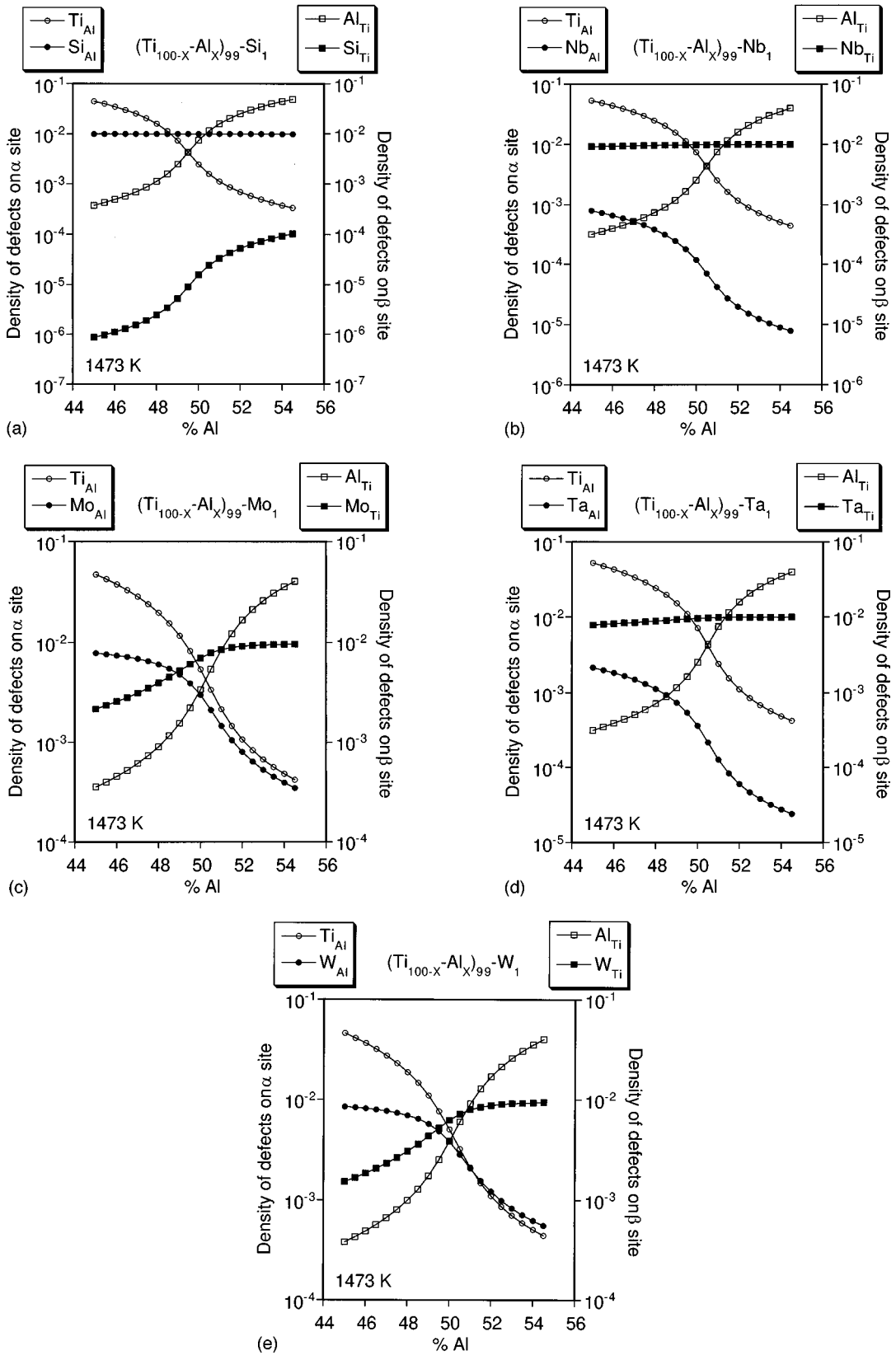

FIG. 5. Predicted point defect densities, at 1473 K, as a function of stoichiometry for ternary elements Si, Nb, Mo, Ta, and W.

stitutional defects, have been calculated using a plane-wave-pseudopotential method. The nearest-neighbor atomic positions were relaxed according to the calculated Hellmann-Feynman forces. The resulting point defect energies were used in a thermodynamic model to predict the formation energy and density of constitutional and thermal point defects as a function of stoichiometry and temperature. Predicted consitutional defects are consistent with experimental observations for the binary alloy. Site selection for the ternary elements are in excellent agreement with the recent work of

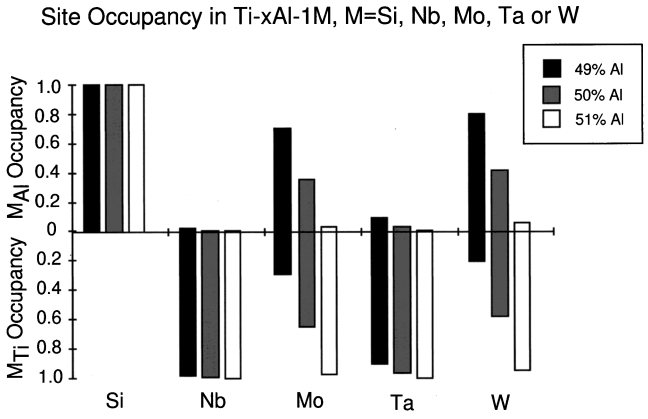

FIG. 6. Predicted sublattice site selection, at 1273 K, of the ternary elements as a function of stoichiometry.

Rossouw *et al.*[42] Predicting the site selection of solid solutions in these alloys is the first step to developing models of solution strengthening based on first-principles methods. Size and modulus misfit parameters can now be calculated for the expected point defects and the results applied in models of solid solution strengthening.

ACKNOWLEDGMENTS

The authors thank S. Rao, D.M. Dimiduk, P.R. Subramanian, and T. A. Partharasarthy for many useful discussions. C.W. also thanks C.J. Rossouw, C.T. Forwood, M.A. Gibson, and P.R. Miller for allowing their results to be used in this paper and for detailed discussions regarding the experimental data. This work was supported by the Air Force Office of Scientific Research and was performed at the Materials and Manufacturing Directorate, Air Force Research Laboratory, Wright-Patterson Air Force Base under Contract Nos. F33615-91-C-5663 and F33615-96-C-5258. This work was supported in part by a grant of HPC time from the DOD HPC centers: CEWES CRAY-YMP, ASC CRAY-C90, and NAVO CRAY-T90.

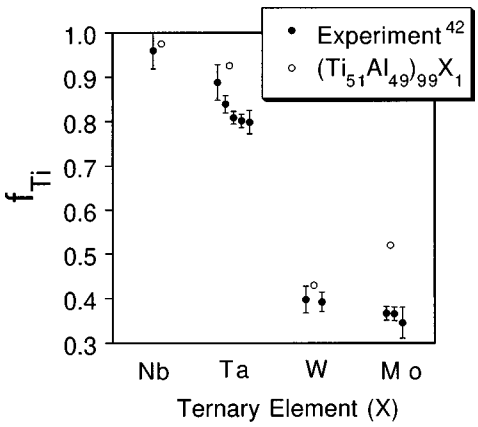

FIG. 7. Comparison of the predicted site occupancy and the experimental observations of Rossouw *et al.*; f_{Ti} is the fraction of ternary atoms occupying Ti sublattice sites.

APPENDIX A: EVALUATION OF C_{ij} USING $\sigma(\epsilon_{ij})$

In the reduced scheme the relation between stress and strain can be written

$$\begin{bmatrix}\sigma_{11}\\ \sigma_{22}\\ \sigma_{33}\\ \sigma_{23}\\ \sigma_{31}\\ \sigma_{33}\end{bmatrix}=C_{ij}\begin{bmatrix}\epsilon_{11}\\ \epsilon_{22}\\ \epsilon_{33}\\ \epsilon_{23}\\ \epsilon_{31}\\ \epsilon_{33}\end{bmatrix}\quad or\quad \begin{bmatrix}\sigma_1\\ \sigma_2\\ \sigma_3\\ \sigma_4\\ \sigma_5\\ \sigma_6\end{bmatrix}=C_{ij}\begin{bmatrix}\epsilon_1\\ \epsilon_2\\ \epsilon_3\\ \epsilon_4\\ \epsilon_5\\ \epsilon_6\end{bmatrix}. \tag{A1}$$

For crystals with cubic symmetry $C_{11}=C_{22}=C_{33}$, $C_{12}=C_{13}=C_{23}$, $C_{44}=C_{55}=C_{66}$, with all other $C_{ij}=0$. For a tetragonal unit cell, such as that needed for $L1_0$ TiAl $C_{11}=C_{22}$, $C_{44}=C_{55}$, $C_{13}=C_{23}$ with all other C_{ij} except C_{33}, C_{66}, and C_{12} set equal to zero. Define a strain tensor ϵ that will transform the lattice vectors to the strained coordinate system

$$\mathbf{a_i'}=\mathbf{a_i}(\mathbf{I}+\epsilon).$$

Here $\mathbf{I}$ is the identity matrix and ϵ is the strain tensor consisting of the nonrotating strains.

$$\epsilon=\begin{pmatrix}\epsilon_1 & \epsilon_6/2 & \epsilon_5/2\\ \epsilon_6/2 & \epsilon_2 & \epsilon_4/2\\ \epsilon_5/2 & \epsilon_4/2 & \epsilon_3\end{pmatrix}. \tag{A2}$$

The C_{ij} for Si and the simple bcc metals were calculated using a strain tensor with $\epsilon_1=\epsilon_2=\epsilon_4=\delta$. For TiAl two calculations were used, one with $\epsilon_1=\epsilon_2=\epsilon_6$ and a second with $\epsilon_1=\epsilon_2=\epsilon_4$. For all these calculations a δ of 0.2% strain was employed. The resulting stress tensors combined with the equilibrium stress tensor are then used with Eq. (A1) to determine the elastic constants.

APPENDIX B: DENSITY OF THERMAL DEFECTS

The grand potential of a binary compound with only intrinsic point defects can be written

$$\frac{\Omega}{N}=\frac{E_0}{N}+n_\alpha^v E_\alpha^v+n_\beta^v E_\beta^v+n_\alpha^B E_\alpha^B+n_\beta^A E_\beta^A-TS$$
$$-\left(\frac{1}{2}-n_\alpha^v+n_\beta^A-n_\alpha^B\right)\mu_A-\left(\frac{1}{2}-n_\beta^v+n_\alpha^B-n_\beta^A\right)\mu_B, \tag{B1}$$

where E_0 is the total energy of the stoichiometric crystal, N is the total number of sites, S is the configurational entropy, and μ_A and μ_B are the chemical potentials. The subscripts and superscripts denote the sublattice (α or β) and species occupying that site A, B, or vacancy (V). E_x^y are the energy differences between the perfect crystal and a crystal containing one defect as denoted by the superscript and subscript. N_x^y and n_x^y are the number and number density of the particular defect (e.g., $n_\alpha^V=N_\alpha^V/N$). For this discussion, it is assumed that there are an equal number of A and B sites, consistent with the $L1_0$ lattice.

The configurational entropy is proportional to the natural log of the number of possible arrangements of the atoms on the sites:

$$S=k_B \ln\left[\frac{(N/2)!}{N_\alpha^A!N_\alpha^B!N_\alpha^V!}\frac{(N/2)!}{N_\beta^B!N_\beta^A!N_\beta^V!}\right]. \tag{B2}$$

From the Stirling formula, $\ln N!\approx N\ln N-N$, for large N, and, the configurational entropy of the A sites can be rewritten

$$\begin{aligned}\ln\left(\frac{(N/2)!}{N_\alpha^A!N_\alpha^B!N_\alpha^V!}\right)&\approx(N/2)\ln(N/2)\\&\quad-N_\alpha^A\ln N_\alpha^A-N_\alpha^B\ln N_\alpha^B-N_\alpha^V\ln N_\alpha^V\\&=-N_\alpha^A\ln(2n_\alpha^A)-N_\alpha^B\ln(2n_\alpha^B)\\&\quad-N_\alpha^V\ln(2n_\alpha^V),\end{aligned} \tag{B3}$$

where the fact $N_\alpha^A+N_\alpha^B+N_\alpha^V=N/2$ has been used.

The grand potential can be rewritten as

$$\begin{aligned}\frac{\Omega}{N}&=\frac{E_0}{N}+n_\alpha^VE_\alpha^V+n_\beta^VE_\beta^V+n_\alpha^BE_\alpha^B+n_\beta^AE_\beta^A\\&\quad+kT[n_\alpha^A\ln(2n_\alpha^A)+n_\alpha^B\ln(2n_\alpha^B)+n_\alpha^V\ln(2n_\alpha^V)\\&\quad+n_\beta^B\ln(2n_\beta^B)+n_\beta^A\ln(2n_\beta^A)+n_\beta^V\ln(2n_\beta^V)]\\&\quad-\left(\frac{1}{2}-n_\alpha^V+n_\beta^A-n_\alpha^B\right)\mu_A-\left(\frac{1}{2}-n_\beta^V+n_\alpha^B-n_\beta^A\right)\mu_B.\end{aligned} \tag{B4}$$

Minimization of the grand potential with respect to the different defect concentrations yields expressions relating the defect concentrations to the chemical potentials and the defect energies. For antisites and vacancies on the α sublattice this gives

$$n_\alpha^B=n_\alpha^Ae^{-\beta[E_\alpha^B-(\mu_B-\mu_A)]}, \tag{B5}$$

$$n_\alpha^V=n_\alpha^Ae^{-\beta(E_\alpha^V+\mu_A)}, \tag{B6}$$

where $\beta=(kT)^{-1}$, and

$$n_\alpha^A=\frac{1}{2}-n_\alpha^V-n_\alpha^B \tag{B7}$$

has been used to define the partial derivatives of these number densities with respect to the number densities of the defects (e.g., $\partial n_\alpha^A/\partial n_\alpha^V=-1$). Expressions for the density of defects on the β sublattice can be obtained in a similar manner using

$$n_\beta^B=\frac{1}{2}-n_\beta^V-n_\beta^A. \tag{B8}$$

Equations (B5) and (B6) can be used with Eq. (B7) to solve for n_α^A:

$$n_\alpha^A=\frac{1}{2}\frac{1}{1+e^{-\beta[E_\alpha^B+(\mu_A-\mu_B)]}+e^{-\beta(E_\alpha^V+\mu_A)}}. \tag{B9}$$

An analogous expression for n_β^B can be found using the the expressions for the defect densities on the β sublattice and Eq. (B8). Using Eq. (B9) in Eqs. (B5) and (B6) gives the number density of the point defects on the α sublattice in terms of the chemical potentials and the defect energies:

$$n_\alpha^V=\frac{e^{-\beta(E_\alpha^V+\mu_A)}}{2Z,}, \tag{B10}$$

$$n_\alpha^B=\frac{e^{-\beta[E_\alpha^B+(\mu_A-\mu_B)]}}{2Z}, \tag{B11}$$

where

$$Z=1+e^{-\beta(E_\alpha^V+\mu_A)}+e^{-\beta[E_\alpha^B+(\mu_A-\mu_B)]}. \tag{B12}$$

Analogous expressions for n_β^A and n_β^V are derived in a similar manner.

For a ternary alloy the grand potential needs to incorporate an additional chemical potential, substitutional defect energies for the ternary on each sublattice, and the number densities of the ternary defects [see Eqs. (2) and (3)]. After including terms for the number of ternary defects in the configurational entropy derivation of the expressions for n_α^C and n_β^C is straighforward using the preceeding arguments. In the ternary case the number densities for the defects take the form

$$n_\alpha^V=\frac{e^{-\beta(E_\alpha^V+\mu_A)}}{2Z}, \tag{B13}$$

$$n_\alpha^B=\frac{e^{-\beta[E_\alpha^B+(\mu_A-\mu_B)]}}{2Z}, \tag{B14}$$

$$n_\alpha^C=\frac{e^{-\beta[E_\alpha^C+(\mu_A-\mu_C)]}}{2Z}, \tag{B15}$$

where

$$Z=1+e^{-\beta(E_\alpha^V+\mu_A)}+e^{-\beta[E_\alpha^B+(\mu_A-\mu_B)]}+e^{-\beta[E_\alpha^C+(\mu_A-\mu_C)]}. \tag{B16}$$

Analogous expressions for n_β^V, n_β^A, and n_β^C are derived as before.

*Also at Materials Research Division, UES Inc., 4401 Dayton-Xenia Rd., Dayton, OH 45432.

[1] K. D. Brommer, M. Needels, B. E. Larson, and J. D. Joannopoulos, Phys. Rev. Lett. **68**, 1355 (1992).

[2] G. Galli, R. M. Martin, R. Car, and M. Parrinello, Phys. Rev. B **42**, 7470 (1985).

[3] T. A. Arias and J. D. Joannopoulos, Phys. Rev. Lett. **73**, 680 (1994).

[4] R. Benedek, L. H. Yang, C. Woodward, and B. I. Min, Phys. Rev. B **45**, 2607 (1992).
[5] A. F. Wright and S. R. Atlas, Phys. Rev. B **50**, 15 248 (1994).
[6] S. Ogut and K. M. Rabe, Phys. Rev. B **50**, 2075 (1994).
[7] J. Hafner, *From Hamiltonians to Phase Diagrams*, Vol. 70 of Solid State Sciences (Springer-Verlag, Berlin, 1987), p. 239.
[8] Y. Kim, JOM **46**, 30 (1994).
[9] D. M. Dimiduk, D. B. Miracle, Y-W. Kim, and M. G. Mendiratta, ISIJ Int. **31** 1222 (1991).
[10] M. P. Teter, M. C. Payne, and D. C. Allan, Phys. Rev. B **40**, 12 255 (1989).
[11] N. Troullier and Jose Luis Martins, Phys. Rev. B **43**, 1993 (1991).
[12] L. Kleinman and D. M. Bylander, Phys. Rev. Lett. **48**, 1425 (1982).
[13] C.-L. Fu and K.-M. Ho, Phys. Rev. B **28**, 5480 (1983).
[14] H. J. Monkhorst and J. D. Pack, Phys. Rev. B **13**, 5188 (1976).
[15] D. M. Ceperley and B. J. Adler, Phys. Rev. Lett. **45**, 566 (1980).
[16] J. P. Perdew and A. Zunger, Phys. Rev. B **23**, 5048 (1981).
[17] F. D. Murnaghan, Proc. Natl. Acad. Sci. USA **30**, 244 (1944).
[18] O. H. Nielsen and R. M. Martin, Phys. Rev. Lett. **50**, 697 (1983).
[19] O. H. Nielsen and R. M. Martin, Phys. Rev. B **32**, 3780 (1985).
[20] In-Ho Lee, Sun-Ghil Lee, and K. J. Chang, Phys. Rev. B **51**, 14 697 (1995).
[21] M. J. Mehl, B. M. Klein, and D. A. Papaconstatopoulos, in *Intermetallic Compounds: Principles and Applications*, edited by J. H. Westbrook and R. L. Fleischer (Wiley, New York, 1994).
[22] C. L. Fu and M. Yoo, in *Alloy Phase Stablity and Design*, edited by G. M. Stocks, D. P. Pope, and A. F. Giamei (Materials Research Society, Pittsburgh, 1991).
[23] A. J. Freeman (private communication).
[24] Y. He, R. B. Schwarz, and A. Migliori, J. Mater. Res. **10**, 1187 (1995).
[25] *Pearson's Handbook of Crystallographic Data for Intermetallic Phases*, edited by P. Villars and L.D. Calvert (American Society for Metals, Metals Park, OH, 1985), Vol 2.
[26] K. Tanaka, T. Ichitsubu, H. Iniu, M. Yamaguchi, and M. Koiwa, Philos. Mag. Lett. **73**, 71 (1996).
[27] C_{44} is determined using two calculations, one with a strain (1-ϵ_4) and a second calculation with atomic displacements along $\langle 111 \rangle$. This procedure is decribed in O. H. Nielsen and R. M. Martin, Phys. Rev. B **32**, 3792 (1985). Alternatively, C_{44} can be determined by relaxing the internal stress by minimizing the Hellmann-Feynman forces of the strained calculation.
[28] M. Sigalas, D. A. Papaconstantopoulos, and N. C. Bacalis, Phys. Rev. B **45**, 5777 (1992).
[29] V. Ozolins and M. Korling, Phys. Rev. B **48**, 18 304 (1993).
[30] W. B. Pearson, *Handbook of Lattice Spacing and Structures of Metals II* (Pergamon, New York, 1967), Vol. 2.
[31] *Single Crystal Elastic Constants and Calculated Aggregate Properties: A Handbook*, edited by G. Simmons and H. Wang (MIT Press, Cambridge, MA, 1971).
[32] J. Wills (private communication).
[33] C. L. Fu and M. Yoo, Philos. Mag. Lett. **62**, 159 (1990).
[34] C. Woodward, J. M. MacLaran, and S. Rao, J. Mater. Res. **7**, 1735 (1992).
[35] U. Brossmann, R. Wurschum, K. Badura, and H.-E. Schaefer, Phys. Rev. B **49**, 6457 (1994).
[36] M. J. Elliot and W. Rostoker, Acta Metall. **2**, 884 (1954).
[37] J. Mayer, C. Elsasser, and M. Fahnle, Phys. Status Solidi B **191**, 283 (1995).
[38] Y. Mishin and D. Farkas, Philos. Mag. A **75**, 169 (1997).
[39] M. Hagen and M. Finnis, Mater. Sci. Forum **207-209**, 245 (1996).
[40] C. L. Fu, Y.-Y. Ye, M. H. Yoo, and K. M. Ho, Phys. Rev. B **48**, 6712 (1993).
[41] S. M. Foiles and M. S. Daw, J. Mater. Res. **2**, 1 (1987).
[42] C. J. Rossouw, C. T. Forwood, M. A. Gibson, and A. R. Miller, Philos. Mag. A **74**, 77 (1996).
[43] F. Zhang, S.-L. Chen, and Y. A. Chang, in *Gamma Titanium Alluminides*, edited by Y-W. Kim, R. Wagner, and M. Yamaguchi (The Minerals, Metals and Materials Society, Pittsburg, PA, 1995), pp. 131–140.
[44] H. Okamoto, J. Phase Equilib. **14**, 120 (1993).
[45] P. A. McQuay, D. M. Dimiduk, H. A. Lipsitt, and S. L. Semiatin, in *Titanium '92 Science and Technology*, edited by F. H. Froes and I. Caplan (The Minerals, Metals and Materials Society, Warrendale, PA, 1993), pp. 387–398.